JOURNAL OF COMPUTATIONAL PHYSICS 112, 173–181 (1994)

Steady Viscous Flow in a Triangular Cavity

CALVIN J. RIBBENS, LAYNE T. WATSON

Department of Computer Science, Virginia Polytechnic Institute & State University, Blacksburg, Virginia 24061

AND

C.-Y. WANG

Departments of Mathematics and Mechanical Engineering, Michigan State University, East Lansing, Michigan 48824

Received June 19, 1992; revised June 28, 1993

Steady recirculating viscous flow inside an equilateral triangular cavity is generated by translating one side. The Navier–Stokes equations are solved numerically using finite differences on a transformed geometry. Alternative numerical approaches, and associated numerical difficulties, are also discussed. The results show a primary eddy and a series of secondary eddies at the stagnant corner. For high Reynolds numbers the interior of the primary eddy has constant vorticity, but its value cannot be predicted by the mean-squared law.

1. INTRODUCTION

Steady recirculating flow is a basic phenomenon in fluid mechanics. Such flows occur in the near wake of moving bluff bodies, in channel flows with abrupt constrictions, or inside cavities partially bounded by solid surfaces. The most studied case in the literature is the cavity flow, a viscous fluid enclosed by solid boundaries except for a translating segment which drives the recirculation through shear stress. This type of flow is important not only in its own right as a basic physical model, but due to its simple geometry, it serves also as a test problem for numerical algorithms.

Not surprisingly, the most widely used geometry for recirculating cavity flow in the literature is a two-dimensional square enclosure with one side translating with uniform velocity. Experimental observations of the streamlines were recorded by Mills [1] and Pan and Acrivos [2] for Reynolds number, defined as (translation velocity) × width/(kinematic viscosity), up to order of 1000. Due to the extreme nonlinearity of the Navier–Stokes equations, little analytic work can be done. In the limit of infinite Reynolds number, Batchelor [3] predicted analytically that the interior would attain constant vorticity given by a mean squared law. A variety of methods are used to solve the problem numerically—finite differences, false transients, finite elements, spectral methods, multigrid methods, etc. (e.g., Burggraf [4], Tuann and Olson [5], Ghia *et al.* [6], Schreiber and Keller [7], Napolitano and Pascazio [8], Shyy *et al.* [9], Iliev *et al.* [10]). It is generally agreed that there is a dominant recirculation whose center is closer to the moving wall. As the Reynolds number is increased, this center first moves downstream, then moves towards the middle of the square. There are two small counter recirculating eddies at the stagnant corners. The vorticity is most intense near the moving boundary. For high Reynolds numbers the vorticity is confined to a boundary layer and the interior vorticity is approximately constant.

However, there are also some differences in the numerical results for the square cavity. The existence of a third small counter rotating eddy upstream of the moving plate has not been accepted by all numerical researchers, nor was it observed experimentally. The numerical scheme of Benjamin and Denny [11] showed enlargement of the small eddies as the Reynolds number is increased, opposite to the conclusion of others. There is also extreme difficulty in increasing the Reynolds number to the extent that Batchelor's theoretical mean-square law [3] can be convincingly confirmed. Finally Schreiber and Keller [12] showed that a computational mesh not sufficiently small would lead to spurious solutions, implicating many earlier numerical calculations may be erroneous.

Also relevant to our work, although less so than the square cavity problem, is the large body of research on unbounded flows over various geometries. For example, Roache [13] discusses flow over a backstep at some length and briefly mentions flow over a triangular notch as well.

The present paper studies numerically the triangular cavity, which to our knowledge has not been done before. This problem is important and interesting in its own right. In fact, the triangular shape is at least as common in practice as the square, since a triangular groove, which is wider

0021-9991/94 $6.00

at the opening, is easier to mill than a square one. A triangular groove is also more common than a square groove on surfaces which have been roughened by scoring. Furthermore, the study of triangular grooves is extremely important in the design of fluid flow across corrugated boundaries. Such corrugations are required due to flexibility [14] or the enhancement of heat transfer [15]. Our aim is to determine the structure of the recirculating flow and the numerical difficulties peculiar to the triangular geometry.

2. FORMULATION

Let Ω be the equilateral triangle with corners $(-\sqrt{3}\,a, a)$, $(\sqrt{3}\,a, a)$, and $(0, -2a)$, and let $\partial\Omega$ be the boundary of Ω. The two-dimensional steady Navier–Stokes equations are

$$u'u'_{x'} + v'u'_{y'} = -\frac{1}{\rho}\,p'_{x'} + \nu(u'_{x'x'} + u'_{y'y'}), \tag{1}$$

$$u'v'_{x'} + v'v'_{y'} = -\frac{1}{\rho}\,p'_{y'} + \nu(v'_{x'x'} + v'_{y'y'}), \tag{2}$$

$$u'_{x'} + v'_{y'} = 0. \tag{3}$$

Here u', v' are velocity components in the Cartesian x', y' directions, ρ is the density, p' is the pressure, and ν is the kinematic viscosity. The boundary conditions are no slip on the sides of the triangle moving with a velocity of constant magnitude U; on fixed sides the velocity is zero; and velocities are bounded inside Ω. We normalize all velocities by U, the pressure by ρU^2, the lengths by a, and we drop the primes. Define a stream function ψ by

$$u = \psi_y, \qquad v = -\psi_x. \tag{4}$$

The governing equations in Ω become

$$\nabla^4\psi = R(\psi_y \nabla^2\psi_x - \psi_x \nabla^2\psi_y), \tag{5}$$

where ∇^2 is the Laplacian operator and R is the Reynolds number Ua/ν. The boundary conditions become

$$\psi = 0 \qquad \text{on all three sides of } \Omega, \tag{6}$$

and

$$(\psi_y, -\psi_x)\cdot\mathbf{T} = \begin{cases} 1 & \text{for the top side,} \\ 0 & \text{for the other two sides,} \end{cases} \tag{7}$$

where $\mathbf{T}$ is a unit vector tangent to the boundary pointing in the direction of motion (clockwise). Equation (7) determines the magnitude of the velocity vector $(\psi_y, -\psi_x)$. The direction of the velocity is already determined (up to the sign) by (6), since $\psi = 0$ on $\partial\Omega$ implies $\nabla\psi = (\psi_x, \psi_y)$ is normal to a side; and thus the velocity, which is normal to $\nabla\psi$, must be tangent to the boundary. For the equilateral triangle Ω considered here, Eq. (7) can be written

$$\begin{aligned} \psi_y &= 1, && \text{on the top side,} \\ \sqrt{3}\,\psi_x - \psi_y &= 0, && \text{on the right side,} \\ \sqrt{3}\,\psi_x + \psi_y &= 0, && \text{on the left side.} \end{aligned} \tag{8}$$

3. NUMERICAL METHODS

We apply a Newton-like iteration to Eq. (5). It is well known that if Newton's method converges to the root of a nonlinear equation, it does so rapidly. However, a good initial guess is usually needed for convergence to occur. We use a very simple initial guess, namely a cubic polynomial constructed to be zero on $\partial\Omega$. For the equilateral triangle we choose

$$\psi^{(0)}(x, y) = -(y-1)(\sqrt{3}\,x + y + 2)(\sqrt{3}\,x - y - 2), \tag{9}$$

while for the right triangle discussed in Section 3.1 below we use

$$\psi^{(0)}(x, y) = xy(x + y - 2\sqrt{3}). \tag{10}$$

Rapid convergence is achieved for $R = 1$ with sufficiently fine grids. Solutions for higher Reynolds number are computed by using as initial guess a solution for a slightly smaller R.

A Newton-like linearization of the nonlinear operator in Eq. (5) results in the linear fourth-order PDE to be solved at each iteration,

$$\begin{aligned} \nabla^4\psi - R(\psi_y^{(i)}\nabla^2\psi_x + \nabla^2\psi_x^{(i)}\psi_y - \psi_x^{(i)}\nabla^2\psi_y - \nabla^2\psi_y^{(i)}\psi_x) \\ = -R(\psi_y^{(i)}\nabla^2\psi_x^{(i)} - \psi_x^{(i)}\nabla^2\psi_y^{(i)}), \end{aligned} \tag{11}$$

where $\psi^{(i)}$ is the approximate solution from the previous step. The linearization is derived by simply expanding the nonlinear operator about some known function and by keeping only the first two terms. See Ribbens *et al.* [16] for a more detailed derivation of (11). At each step of the outer iteration we must solve the linear problem defined by Eqs. (6), (8), and (11). Note that linearization precedes discretization. One could also discretize first and then deal with the resulting system of nonlinear equations, but the two approaches are essentially equivalent.

3.1. *Finite Differences on Original Problem*

An efficient numerical technique for solving the related driven square cavity problem is described by Schreiber and

Keller [7]. The technique employed in [7] is based on central differences and a uniform rectangular grid, yielding a discretization with second-order accuracy. The difference formulas used to approximate the derivative terms in both the PDE and the boundary conditions are centered. A 13-point stencil is required for the fourth-order derivatives. In order to impose the PDE at grid points just inside the region, "fictitious" grid points just exterior to the boundary are required, but the unknown ψ values at these exterior grid points are determined by imposing the normal derivative boundary condition at nearby boundary grid points. The technique in [7] also includes continuation in the Reynolds number, a special sparse direct factorization scheme for the resulting linear systems, and Richardson extrapolation for improved accuracy.

We considered modifying the approach of Schreiber and Keller for the triangle problem. Unfortunately, the equilateral triangle presents considerable difficulties under such an approach. Figure 1 shows a typical case. As in Ref. [7], we introduce grid points just external to the region. Each external point above the top edge is eliminated by imposing the derivative boundary condition (8) at the boundary grid point directly beneath it. The unknown value at an external grid point along the left or right side is determined by imposing the derivative boundary condition at the boundary grid point immediately above that point. Centered formulas are used for the derivatives in these boundary conditions for all but two points. Note that no external points are defined just above or below the upper left and right corners. The reason is that introducing such points would immediately lead to a singular system, since

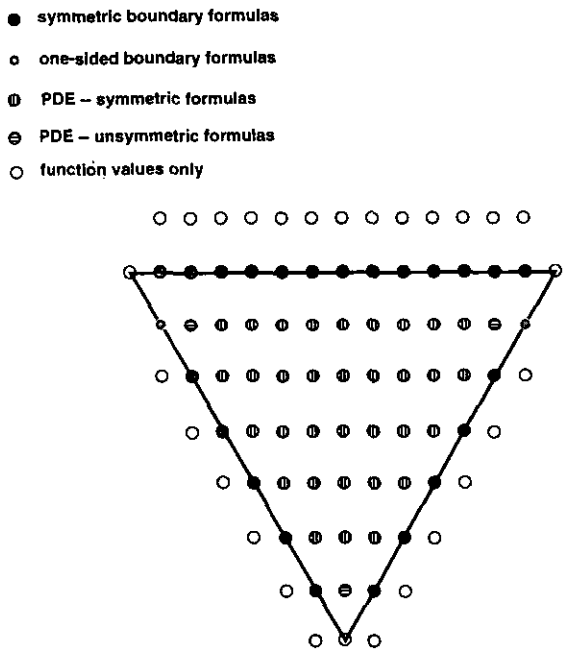

FIG. 1. Equations and unknowns for the equilateral triangle Ω.

there is only one nearby boundary point (the corner itself) at which to enforce boundary conditions, but we would have two new fictitious points. Furthermore, the derivative boundary conditions are not well defined at the corners, so imposing them in an arbitrary direction seems dangerous. Similarly, we do not have an external grid point beneath the bottom corner because the derivative boundary condition is not defined at the corner. The immediate result of this special treatment near the corners is that we must use nonsymmetric stencils for the x derivatives at the boundary grid points nearest the two upper corners, and we must use nonsymmetric 18-point stencils for the PDE at the interior points nearest all three corners. For the remaining interior grid points the standard 13-point finite difference stencil suffices.

Unfortunately, our relatively straightforward generalization of the technique of Schreiber and Keller resulted in linear systems which are so ill conditioned that accurate numerical solutions are virtually impossible. In fact, for moderately fine grids (e.g., 49 vertical grid lines and 25 horizontal grid lines) the systems are numerically singular, with condition numbers in excess of 10^{13}. The problem is related to the special treatment required in the corners and to the overlapping stencils needed for the derivative boundary equations along the left and right sides. On a test problem, if we assume the external solution values are known, so that neither the one-sided stencils nor the derivative boundary equations are needed, the linear systems become quite well conditioned (e.g., 10^3 for the case mentioned above). We did not pursue further the causes of the ill conditioning or seek remedies, as the approach described in the next section proved successful. However, it is interesting to note the significant problems that arise in modifying the straightforward difference method of Schreiber and Keller for the triangle.

3.2. *Other Approaches*

In a previous paper [16] we described a numerical technique for solving the related problem of flow induced in an elliptic region by the boundary moving at constant velocity. In that work our numerical approach was based on collocation with Hermite cubic basis functions, and we defined the problem as a coupled system of two second-order equations in two unknowns (stream function and vorticity). This strategy proved quite successful and yielded accurate solutions for Reynolds number up to 1000 and for ellipses with aspect ratio up to five.

An analogous strategy for the present problem is not successful, however. As in the finite difference method described above, special problems near the corners lead to nearly singular linear systems and, in fact, to exactly singular systems if the collocation points are not chosen carefully. Our experience is that this extreme ill conditioning causes

inaccuracies in the approximate solution and prevents the Newton iteration from converging for all but the smallest Reynolds numbers. Neither collocation nor centered finite differences applied to the system of two second-order equations was successful. A further problem with the stream function-vorticity formulation is that the correct boundary conditions for the vorticity are not clear in this case, since both boundary conditions are in terms of the stream function.

Although our primary emphasis here is on considering various finite difference approaches, in addition to the collocation method mentioned above, we also considered other finite element methods. The triangular geometry suggests that triangular finite elements are an obvious choice, for example. However, high order elements are needed in order to discretize the fourth-order differential operator, and hence the programming effort is still substantial.

3.3. *Finite Differences on a Transformed Problem*

Returning to a direct finite difference treatment of the fourth-order problem, a more successful numerical treatment is possible. The key step is to transform the problem to an equivalent problem posed on a right triangle. In particular, we introduced a change of variables

$$\xi = x + (y+2)/\sqrt{3}, \qquad \eta = 2(1-y)/\sqrt{3},$$

so that our computational region is a right triangle $\tilde{\Omega}$ with corners $(0, 0)$, $(2\sqrt{3}, 0)$, and $(0, 2\sqrt{3})$. The transformed PDE operator in ξ, η is a very general one indeed, since the chain rule produces terms of up to total (derivative) degree four with coefficients depending on the coefficients of the original problem and on the transformation. Deriving the transformed coefficients and new difference formulas for all of these derivative terms by hand would be extremely tedious. We found the process reasonably straightforward, however, using the symbolic computational facilities of Mathematica [17].

The most important benefit of transforming the problem to a right triangle is that the transformed derivative boundary conditions are still simply normal derivative conditions on $\tilde{\psi}$, the unknown in $\tilde{\Omega}$ (i.e., a Neumann condition). This is precisely true only for an equilateral triangle transformed to an isosceles right triangle. The original problem posed on a scalene triangle might be unavoidably ill conditioned—this remains a topic for future work. This Neumann boundary condition is extremely important for the numerical scheme because it allows us to use centered difference formulas to approximate these derivative conditions and because these formulas do not overlap (as they do on the equilateral triangle). As can be seen in Fig. 2, we again introduce unknowns exterior to the region and eliminate them by hand by imposing the derivative boundary condition at the nearest point on the boundary. Note that along the hypotenuse of the triangle we impose the derivative boundary condition at the midpoint of a grid square rather than on a grid point. There are several possibilities for second-order accurate finite difference stencils in the interior of the region. As can be seen in Fig. 3, the stencil we use is skewed so that it "fits" the geometry. Thus, we are able to use the same difference equations to approximate the PDE at all interior points, including those closest to the corners. This is another important benefit of the transformed problem approach. Figure 3 shows the stencil for the PDE applied at the interior grid point closest to the top corner. Other second-order accurate stencils require an extra diagonal of fictitious points along the hypotenuse. The coef-

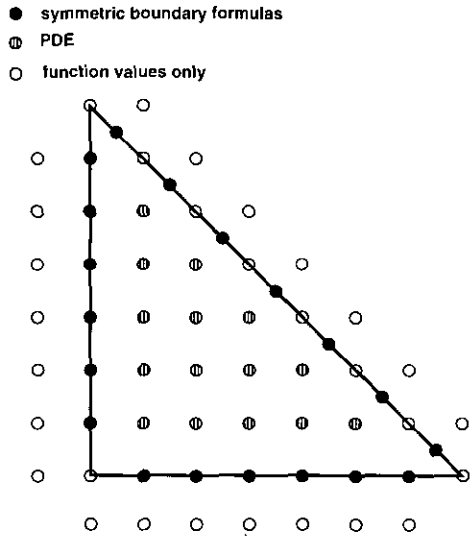

FIG. 2. Equations and unknowns for the right triangle $\tilde{\Omega}$.

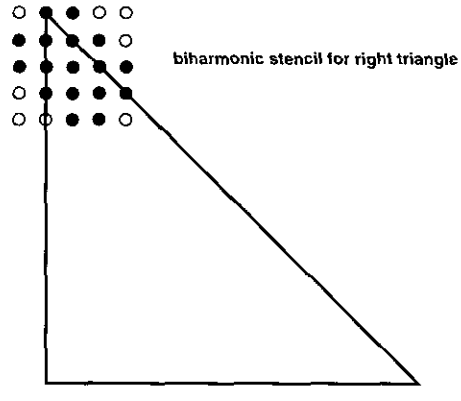

FIG. 3. Stencil for approximating derivatives of up to degree four on the right triangle $\tilde{\Omega}$. The difference equations for the center point involve unknowns at each of the solid circles.

ficients for the various finite difference approximations based on this skewed stencil are given in the Appendix.

The results reported in the next section are based on a 200×200 square mesh. The resulting linear system has 19,701 equations and unknowns. We solve the discrete problem using band Gauss elimination. We obtain solutions for Reynolds numbers 1, 10, 50, 100, 150, 200, 250, 300, 350, 400, 450, 500. Higher Reynolds numbers would require a finer mesh, which in turn would require either more computer memory or a different linear equation solver. Alternatively, an upwind difference scheme might allow solutions for higher Reynolds number, since the cell Reynolds number for our scheme is as high as 15 (values larger than two can lead to stability problems in the time dependent case). In order to have confidence in our solutions, for several Reynolds numbers we also did solutions using coarser meshes (e.g., 50×50 and 100×100). Comparing these results with the finest mesh shows the expected convergence with respect to the mesh size. Care must be taken to avoid spurious solutions for the highest Reynolds numbers, however. Schreiber and Keller [12] show that for a given mesh size, there is a point where increasing the Reynolds number further can lead to spurious solutions. We give an example of such a spurious solution below.

4. RESULTS

Figure 4 shows the streamline patterns as the Reynolds number is increased. The top boundary is translating to the right, driving the recirculation eddy through viscous shear. For $R < 1$ the streamlines are almost symmetric with respect to the y axis. The clockwise primary eddy is about $\frac{4}{5}$ from the bottom vertex and moves downstream (to the right) as R is increased. There are several secondary eddies alternating in sign and rapidly decreasing in strength towards the stagnant corner. According to Moffsatt's analysis, the size ratio of the eddies for a 60° stagnant corner is about 4.8, which is consistent with our results.

Figure 5 shows the corresponding vorticity distribution, defined as $\zeta = \nabla^2 \psi$. In general vorticity is large and positive near the top, and at large Reynolds numbers, it is convected to the right side. Finally at $R = 500$, the vorticity changes become more restricted to the boundaries. Figure 6 shows the vorticity distributions for $R = 500$ along two different directions across the cavity. It is seen that the "interior" of the primary eddy has almost constant vorticity. We define the center (x_c, y_c) of the primary eddy as the location of maximum ψ value in the cavity. Table I shows that as R increases to 500, the location of the center (x_c, y_c), its stream function value ψ_c, and its vorticity ζ_c all seem to have converged. Similar to the case of the square, the primary eddy center first moves toward the right side, then towards the center of the triangle. Now the fact that $R = 500$ does not seem to be large is due to our definition of R. If a side of the triangular cavity is used as the length scale, the actual Reynolds number would be $2\sqrt{3}$-fold, so our $R = 500$ is equivalent to a conventional Reynolds number of 1732.

TABLE I

Properties of the Center of the Primary Eddy, Located at (x_c, y_c) with Stream Function Value ψ_c and Vorticity ζ_c

R	x_c	y_c	ψ_c	ζ_c
1	0.0169	0.460	0.233	1.363
50	0.346	0.445	0.237	1.464
100	0.329	0.355	0.247	1.373
200	0.208	0.280	0.260	1.272
350	0.173	0.265	0.268	1.232
500	0.173	0.265	0.269	1.250

5. DISCUSSION AND CONCLUSIONS

Physically the flow in a triangular cavity is similar to the flow in a square cavity. There is, however, only a single stagnant corner where we find a series of small eddies. This phenomena is also shown experimentally for a triangular cavity with a small opening angle (Van Dyke [18]).

Now let us compute the interior constant vorticity predicted by Batchelor [3]. The analytic solution for inviscid rotational flow with constant vorticity inside an equilateral triangle is given by Eq. (9). Using the mean-square law on the boundary velocity we find the interior vorticity for large R is $\sqrt{10}/3 = 1.054$. This is much lower than our numerical value of 1.250. We conclude that Batchelor's theory does not apply to the triangular cavity. There are several reasons. First, the mean-square law assumes a zero pressure gradient along the boundary. The inviscid flow of Eq. (9), however, shows that pressure rises at the three stagnant corners. Second, the assumption of a thin boundary layer enclosing the primary eddy is violated for the triangle. Figure 5e shows secondary eddies occupying large areas. As Figs. 5a–e show, these secondary eddies seem to become larger as R is increased (also concluded by Benjamin and Denny [11]). Thus the mean-square law is found to be approximately valid for circular or elliptic boundaries (Ribbens *et al.* [16]), may be valid for the square cavity if corner eddies are small, but is not valid for the triangular cavity. An interesting experiment for future work would be to test the mean-square law for trapezoidal shaped cavities (of which the square and triangle are limiting cases), with both one side moving and all sides moving. This problem has been studied for one particular trapezoid by Darr and Vanka [19].

Another difference between the triangular cavity and the square cavity is in the numerical method. Due to the

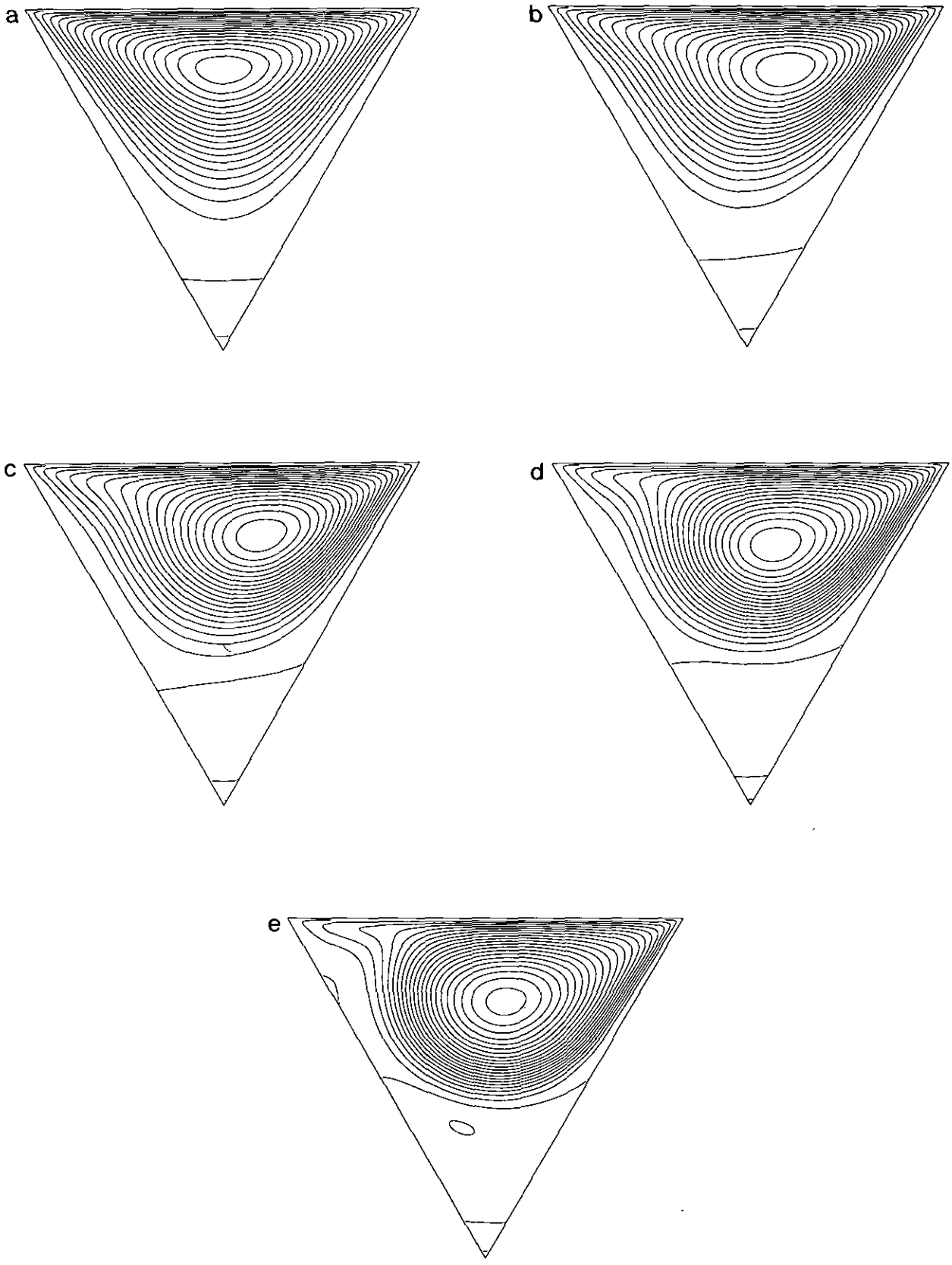

FIG. 4. Streamline patterns for $R = 1$ (a), $R = 50$ (b), $R = 100$ (c), $R = 200$ (d), and $R = 500$ (e).

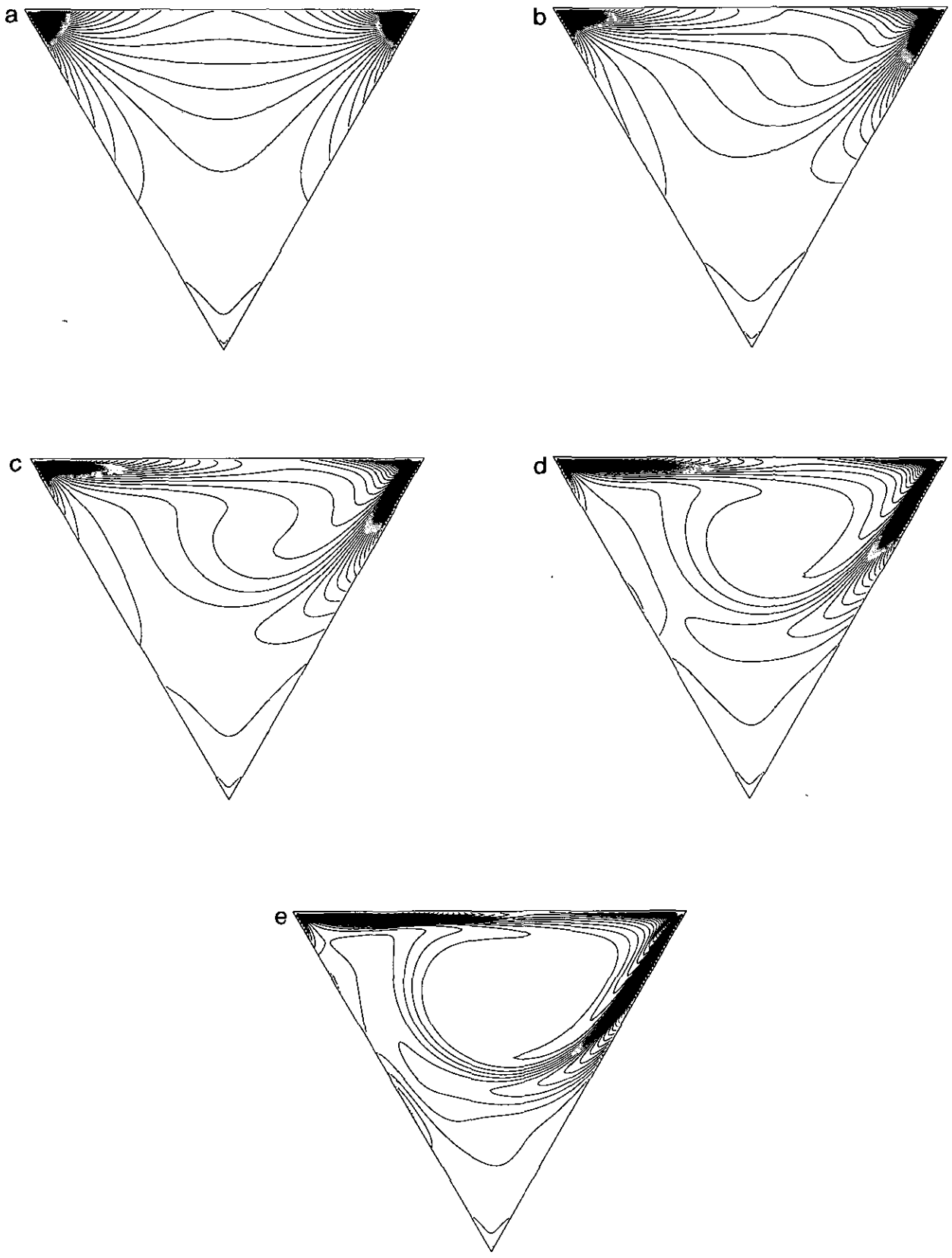

FIG. 5. Vorticity distribution for $R = 1$ (a), $R = 50$ (b), $R = 100$ (c), $R = 200$ (d), and $R = 500$ (e).

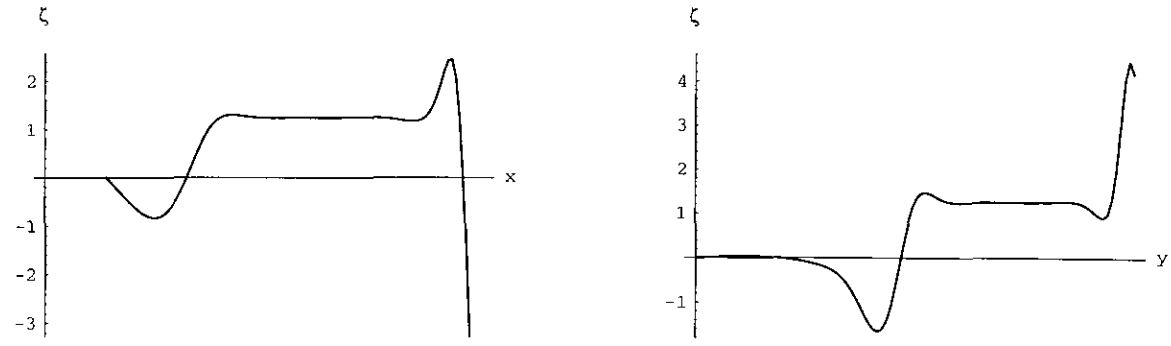

FIG. 6. Vorticity values for $R = 500$ along $y = 0.265$ (left) and along $x = 0.173$ (right).

geometry, especially at the corners, problems arise if standard algorithms are applied directly. We finally transformed the geometry to an isosceles right triangle and successfully applied a finite difference method, although new formulas had to be derived for the asymmetric stencil in Fig. 3. Care must be taken to use a grid size large enough to be efficient computationally and small enough such that spurious solutions are not obtained. An example of a spurious solution is shown in Fig. 7.

APPENDIX

The (i, j) entry in the templates below is the coefficient α_{ij} of $\Psi(x + ih, y + jh)$ in the finite difference approximation $\sum_{i,j=-2}^{2} \alpha_{ij} \Psi(x + ih, y + jh)$ to a particular partial derivative of Ψ at (x, y):

$$\Psi_x : \frac{1}{2h} \begin{bmatrix} & 0 & 0 & & \\ 0 & 0 & 0 & 0 & \\ 0 & -1 & 0 & 1 & 0 \\ & 0 & 0 & 0 & 0 \\ & & 0 & 0 & \end{bmatrix},$$

$$\Psi_y : \frac{1}{2h} \begin{bmatrix} & 0 & 0 & & \\ 0 & 0 & 1 & 0 & \\ 0 & 0 & 0 & 0 & 0 \\ & 0 & -1 & 0 & 0 \\ & & 0 & 0 & \end{bmatrix},$$

$$\Psi_{xx} : \frac{1}{h^2} \begin{bmatrix} & 0 & 0 & & \\ 0 & 0 & 0 & 0 & \\ 0 & 1 & -2 & 1 & 0 \\ & 0 & 0 & 0 & 0 \\ & & 0 & 0 & \end{bmatrix},$$

$$\Psi_{xy} : \frac{1}{4h^2} \begin{bmatrix} & 0 & 0 & & \\ 0 & -1 & 0 & 1 & \\ 0 & 0 & 0 & 0 & 0 \\ & 1 & 0 & -1 & 0 \\ & & 0 & 0 & \end{bmatrix},$$

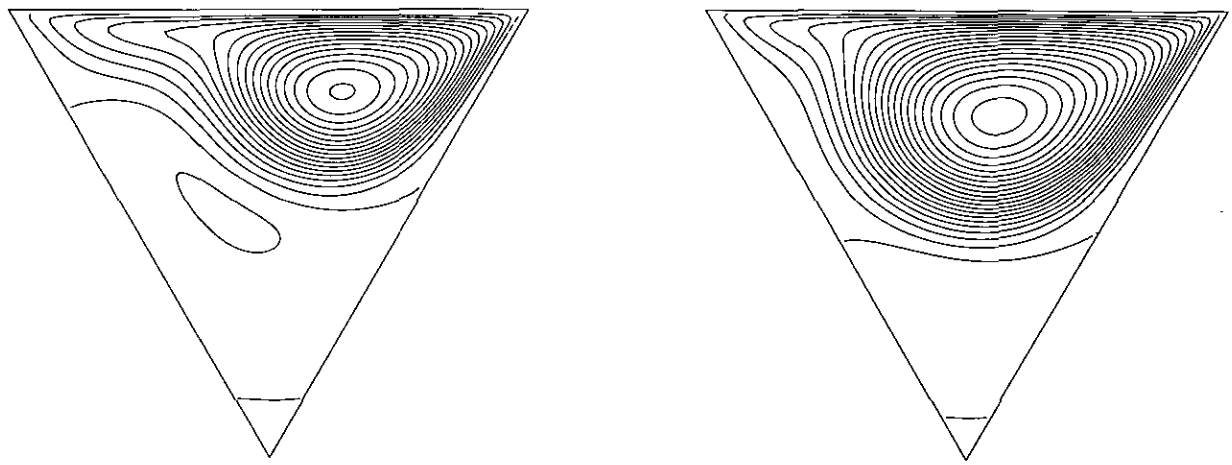

FIG. 7. A spurious solution (left) and the correct solution (right) for $R = 275$.

$$\Psi_{yy}: \frac{1}{h^2}\begin{bmatrix} & 0 & 0 & & \\ 0 & 0 & 1 & 0 & \\ 0 & 0 & -2 & 0 & 0 \\ & 0 & 1 & 0 & 0 \\ & & 0 & 0 & \end{bmatrix},$$

$$\Psi_{xxx}: \frac{1}{2h^3}\begin{bmatrix} & & 0 & 0 & & \\ & 0 & 0 & 0 & 0 & \\ -1 & 2 & 0 & -2 & 1 & \\ & & 0 & 0 & 0 & 0 \\ & & & 0 & 0 & \end{bmatrix},$$

$$\Psi_{xxy}: \frac{1}{2h^3}\begin{bmatrix} & 0 & 0 & & \\ 0 & 1 & -2 & 1 & \\ 0 & 0 & 0 & 0 & 0 \\ & -1 & 2 & -1 & 0 \\ & & 0 & 0 & \end{bmatrix},$$

$$\Psi_{xyy}: \frac{1}{2h^3}\begin{bmatrix} & 0 & 0 & & \\ 0 & -1 & 0 & 1 & \\ 0 & 2 & 0 & -2 & 0 \\ & -1 & 0 & 1 & 0 \\ & & 0 & 0 & \end{bmatrix},$$

$$\Psi_{yyy}: \frac{1}{2h^3}\begin{bmatrix} & 0 & 1 & & \\ 0 & 0 & -2 & 0 & \\ 0 & 0 & 0 & 0 & 0 \\ & 0 & 2 & 0 & 0 \\ & & -1 & 0 & \end{bmatrix},$$

$$\Psi_{xxxx}: \frac{1}{h^4}\begin{bmatrix} & 0 & 0 & & \\ 0 & 0 & 0 & 0 & \\ 1 & -4 & 6 & -4 & 1 \\ & 0 & 0 & 0 & 0 \\ & & 0 & 0 & \end{bmatrix},$$

$$\Psi_{xxxy}: \frac{1}{2h^4}\begin{bmatrix} & & 0 & 0 & & \\ & -1 & 3 & -3 & 1 & \\ & 1 & -4 & 6 & -4 & 1 \\ & & 1 & -3 & 3 & -1 \\ & & & 0 & 0 & \end{bmatrix},$$

$$\Psi_{xxyy}: \frac{1}{h^4}\begin{bmatrix} & 0 & 0 & & \\ 0 & 1 & -2 & 1 & \\ 0 & -2 & 4 & -2 & 0 \\ & 1 & -2 & 1 & 0 \\ & & 0 & 0 & \end{bmatrix},$$

$$\Psi_{xyyy}: \frac{1}{2h^4}\begin{bmatrix} & -1 & 1 & & \\ 0 & 3 & -4 & 1 & \\ 0 & -3 & 6 & -3 & 0 \\ & 1 & -4 & 3 & 0 \\ & & 1 & -1 & \end{bmatrix},$$

$$\Psi_{yyyy}: \frac{1}{h^4}\begin{bmatrix} & 0 & 1 & & \\ 0 & 0 & -4 & 0 & \\ 0 & 0 & 6 & 0 & 0 \\ & 0 & -4 & 0 & 0 \\ & & 1 & 0 & \end{bmatrix}.$$

ACKNOWLEDGMENTS

The work of Calvin J. Ribbens and Layne T. Watson was supported in part by Department of Energy Grant DE-FG05-88ER25068 and Air Force Office of Scientific Research Grant 89-0497. We also thank the referees for their thoughtful comments and suggestions.

REFERENCES

1. R. D. Mills, *J. R. Aeronaut. Soc.* **69**, 116 (1965).
2. F. Pan and A. Acrivos, *J. Fluid Mech.* **28**, 643 (1967).
3. G. K. Batchelor, *J. Fluid Mech.* **1**, 177 (1956).
4. O. R. Burggraf, *J. Fluid Mech.* **24**, 113 (1966).
5. S. Y. Tuann and M. D. Olson, *J. Comput. Phys.* **29**, 1 (1978).
6. U. Ghia, K. N. Ghia, and C. T. Shin, *J. Comput. Phys.* **48**, 387 (1982).
7. R. Schreiber and H. B. Keller, *J. Comput. Phys.* **49**, 310 (1983).
8. M. Napolitano and G. Pascazio, *Comput. Fluids* **19**, 489 (1991).
9. W. Shyy, S. Thakur, and J. Wright, *AIAA J.* **30**, 923 (1992).
10. O. P. Iliev, M. M. Makarov, and P. S. Vassilevski, *Int. J. Numer. Methods Eng.* **33**, 1465 (1992).
11. A. S. Benjamin and V. E. Denny, *J. Comput. Phys.* **33**, 340 (1979).
12. R. Schreiber and H. B. Keller, *J. Comput. Phys.* **49**, 165 (1983).
13. P. J. Roache, *Computational Fluid Dynamics* (Hermosa, Albuquerque, NM, 1972).
14. C. N. Savvides and J. H. Gerrard, *J. Fluid Mech.* **138**, 129 (1984).
15. E. M. Sparrow and M. Charmchi, *Int. J. Heat Mass Trans.* **23**, 471 (1980).
16. C. J. Ribbens, C.-Y. Wang, L. T. Watson, and K. A. Alexander, *Comput. Fluids* **20**, 111 (1991).
17. S. Wolfram, *Mathematica* (Addison-Wesley, Redwood City, CA, 1988).
18. M. Van Dyke, *Album of Fluid Motion* (Parabolic, Stanford, CA, 1982).
19. J. H. Darr and S. P. Vanka, *Phys. Fluids A* **3**, 385 (1991).